Friction **4**(3): 238–248 (2016)
DOI 10.1007/s40544-016-0121-y
ISSN 2223-7690
CN 10-1237/TH

RESEARCH ARTICLE

Effect of surface topography with different groove angles on tribological behavior of the wheel/rail contact using alternative machine

A. KHALLADI[1,2], **K. ELLEUCH**[1,*]

[1] *Laboratory of Materials Engineering and Environment (LGME), National Engineering School of Sfax (ENIS), University of Sfax, Sfax 3038, Tunisia*

[2] *Department of Mechanical, Higher Institutes of Technological Studies of Sfax (ISET SFAX), University of Sfax, Sfax 3099, Tunisia*

Received: 30 March 2016 / Revised: 12 June 2016 / Accepted: 06 July 2016

Abstract: The objective of this study was to investigate the influence of the surface topography on the tribological behavior of the wheel/rail contact. Four different groove orientations forming the surface topographies—smooth surface, 0°, 45° and 90°—were manufactured by grinding and compared. All friction tests with different surface topographies were conducted using an alternative tribometer simulating the pure sliding process in the wheel-rail contact. The Hertzian pressure was maintained at 1,000 MPa with two levels of sliding velocity (20 mm/s and 80 mm/s). This study resulted in five main findings.

First, the initial surface topographies seemed to have a significant effect on the friction coefficient independently of the speed. Second, the increase of the sliding velocity would decrease the friction coefficient. Third, especially when accompanied with a high sliding velocity, an initial rough surface would have a significant effect on the wear of the wheel. Fourth, the highest wear values were observed at groove orientations of 45° when accompanied with a high sliding velocity. Finally, the break-in duration seemed to depend on the initial surface topographies of the rail and the sliding velocity.

Keywords: wheel/rail contact; groove; friction; wear; break-in

1 Introduction

Grinding operation has been used for maintaining optimal rail profile and removing rail surface defects, such as corrugation, checking, plastic flow, spalls and fatigue cracks [1–3]. Eric and Joseph argued that maintaining conform wheel and rail profiles had positive effects on wear, fatigue, corrugation, stability and derailment potential [1]. As was recommended by Cuervo et al., any rail damage must be removed or repaired to improve the security of operation of the rail transportation [2]. In addition, Chandrasekar et al. argued that after grinding procedure a hard layer composed of untempered martensite can be formed at the surface due to localized heating [4]. However, Lyu et al. predicted that surface topographies can be completely changed after grinding operations. Then, using a pure sliding with pin-on-disc configuration, they revealed that surface topographies would result in wear, friction coefficient and noise tension [5]. In the case of wheel–rail contact, the main cause of wear is sliding [5–7]. In another study, Lundmark et al., using a two disc machine, studied the effect of the surface topography of the rail grinding on the running-in period, wear and traction behavior [8]. In their study, these scholars concluded that the surface topographies had an insignificant effect on the running-in period and an unclear effect on the wear and traction coefficient. Moreover, several studies have shown

* Corresponding author: K. ELLEUCH.
E-mail: khaled.elleuch@enis.rnu.tn

that the roughness can be greatly reduced following the passage of traffics [8–10]. Lundermark claimed that the surface roughness was reduced 10 times (10 μm to 1 μm) just after one and half days of a 260,800-ton traffic [8]. Garssie reported that the roughness of the running band changed rapidly following the passage of 43,500 tons—the equivalent of one day's traffic [9]. Hiensch et al. revealed that traces of grinding remained visible even after 6 months of traffic (6.7 MGT) [10].

As can be seen from this review there is little information on surface topography with different groove angles on tribological behavior of wheel/rail contact. For this reason, this study attempted to explore the effect of the initial rail surface topography with various groove orientations on the friction coefficient, break-in, wear and surface damage of the wheels using the alternative machine.

2 Experimental details

2.1 Expertise

This work was conducted within the Research Department of the National Railway Company, Tunisia (SNCFT) in collaboration with the Materials Engineering and Environmental Laboratory (LGME-Tunisia).

Expertise of the Tunisian railway network, line 5—exactly between Chaffar and Mahres stations—undertaken on 27 April 2012 revealed that just after the grinding operation, the typography of the rail was completely changed as can be seen in Fig. 1. Groups of grooves oriented at 0°, 45° and 90° relative to the traffic direction and caused by grinding operation were observed visibly on the active rail surface (rail head and gauge). It is worth mentioning that the mean SNCFT traffic on that line was about 8,000 tons/day. It should be note that many reasons can maintain the grinding marks visible for more than three months like the traffic load, the initial parameters of grinding operation and the environmental effect.

2.2 Samples preparation

The materials used as test samples were cut using a robot-wire machine device from a wheel and a rail chosen randomly. In order to eliminate the decarburized layer and to keep comparable locations, 8-mm samples were extracted from the wheel and rail surfaces, as was shown in previous works [11, 12].

The location zone and the dimensions of the samples are shown in Fig. 2, it should be noted that steel materials of wheel and rail were respectively R7 and 900A. The chemical composition and the mechanical characteristics of R7 and 900A steel are shown in Table 1.

Prior to testing, samples were mechanically polished to 1000 grade paper to obtain a smooth surface with roughness Ra about 0.08 μm. In the second step, three plane surfaces were manufactured using abrasive paper #80 to obtain a rough surface with three different orientation grooves as is shown in Fig. 3. While the surface finish of the pins was kept constant for all tests, the rough surface value for all pin tests was about 0.09 μm. This range of the surface roughness is reported by many studies on the wheel rail contact [5, 6, 13]. The surface roughness was measured using a TAYLOR HOSON SURFTRONIC 25 profilometer. Using cotton soaked in ethyl acetate, the pins and the

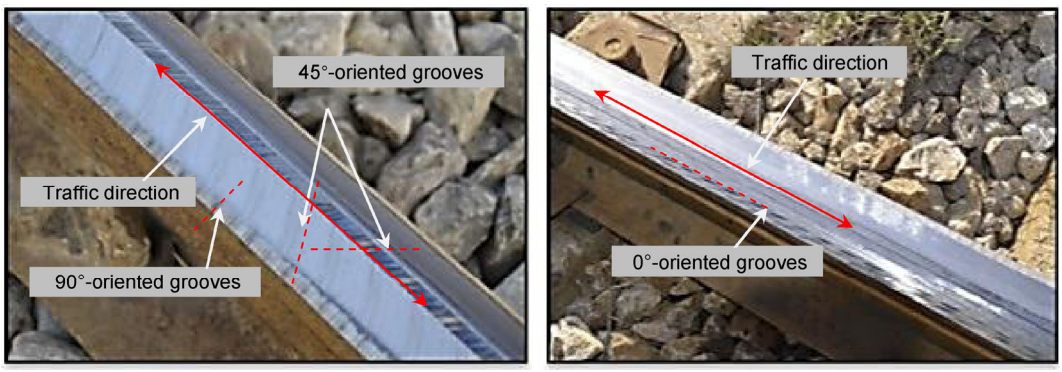

Fig. 1 Expertise just after rail grinding process.

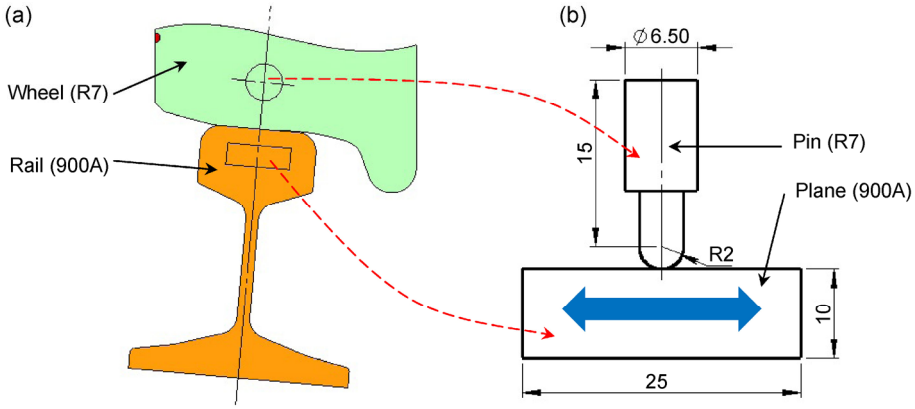

Fig. 2 Sample characterization. (a) location zone and (b) dimensions of the sample in mm.

Table 1 Mechanical properties and chemical composition of the wheel and rail materials.

		R7	900A
Elastic modulus, E (GPa)		210	210
Tensile strength, R_m (MPa)		850	950
Yield strength, $R_{P0,2}$ (MPa)		490	570
Hardness HV30 (GPa)		2.50	2.77
Chemical composition (weight %)			
	C	0.44	0.67
	Cr	0.24	0.03
	Si	0.26	0.29
	Mn	0.76	1.08

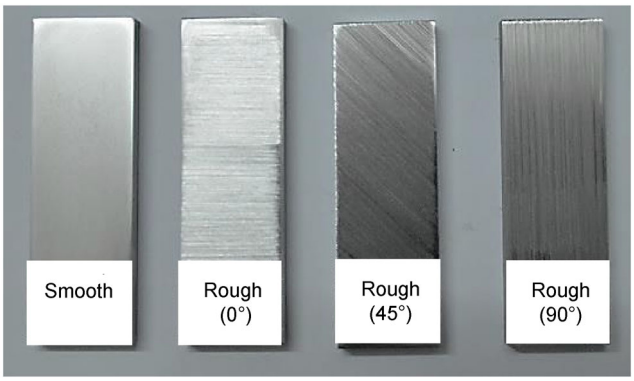

Fig. 3 Photo of the test samples after manufacturing.

discs were cleaned from residues of pollution caused by handling the samples and machine wiping. Then in the second stage, all samples were dipped in an ultrasonic (power Sonic 405) bath of trichloroethylene, at a temperature of 50 °C, for 30 min, to ensure both mechanical and chemical action [14]. The rough surfaces of all planes are shown in Table 2.

Figure 4 shows the optical transversal observation. These photos show the difference between smooth and rough surface morphologies of planes.

2.3 Test apparatus

Figure 5 shows a schematic diagram of alternative tribometer and contact configuration. During test, normal load was kept constant at F_n = 5 N within the contact by applying dead weight. Tangential force (F_t) was recorded continuously and friction curves were obtained by computer system software. The coefficient friction (μ) is the ratio between the tangential force (F_t) and the normal force (F_n). The coefficient friction is as a function of the number of cycles. Tests were performed at 31 °C in laboratory ambient condition at 30% relative humidity.

2.4 Test conditions

A combination of sliding velocity and contact pressure was a wise choice taken from the wear map of wheel/rail. Both sliding velocities (20 mm/s and 80 mm/s) were determined from the wear map of the wheel and rail steels. The chosen sliding velocity represented both limitation zones of rail head/wheel tread studies area [15]. Each test was repeated three times. Each of the four surface topographies (smooth, rough 0°, rough 45° and rough 90°) were tested with two different sliding velocities. All the test results were recorded after 5,000 cycles. Then, it was decided to repeat the tests and stop at the end of the break-in period. This was called "first stage". All in all 48 tests were

Table 2 Plates surface topographies.

Used abrasive paper		#1000	#80		
Sample type		Smooth	Rough (0°)	Rough (45°)	Rough (90°)
Orientation grooves relative to sliding direction					
Ra (μm)	Parallel with sliding direction	0.08	0.24	0.92	1.19
	Perpendicular to sliding direction	0.08	1.84	0.97	0.45

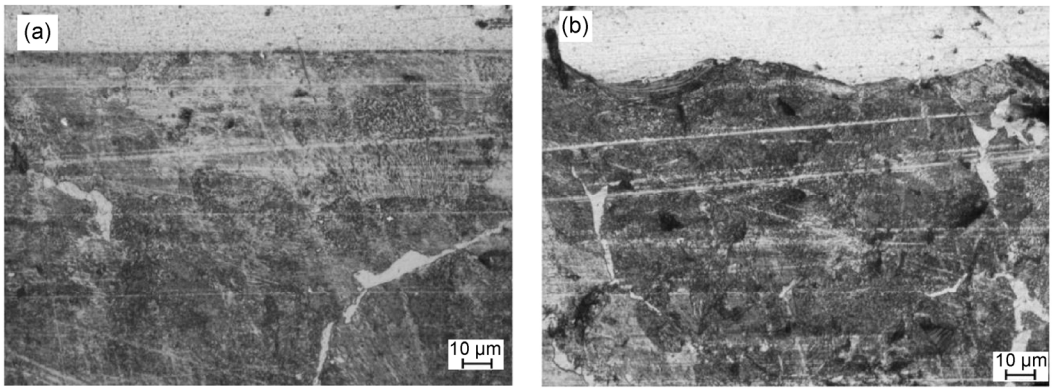

Fig. 4 Optic transverse observation: (a) smooth surface and (b) rough surface.

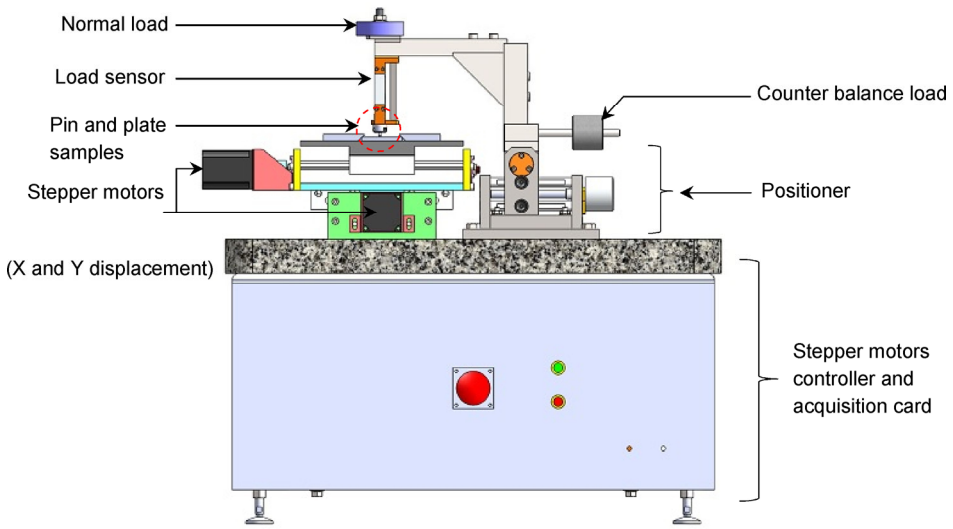

Fig. 5 Schematic diagram of alternative machine.

conducted. The test parameters are shown in Table 3. Pin-on-plane configuration and orientation grooves relative to sliding direction are shown in Fig. 6.

2.5 Wear rate volume measurement

At the end of the test, all pin wear scars had a circular shape. Delamination metallic debris and oxide layer adhered to wear surface of the pin, making it difficult to quantify its wear by the mass loss measurement. Therefore, pins wear rate was calculated with wear volume based on the measurement of the radius wear scar "*r*" (Fig. 7). Therefore, the wear volume can be determined by the wear volume of the spherical cap using Eq. (1).

Table 3 Common parameters for friction tests.

Parameter	Unit	Value
Normal load	N	5
Amplitude	mm	15
Sliding velocity		
V1	mm/s	20
V2	mm/s	80
Number of cycles		5,000
Ambient temperature	˚C	31
Relative humidity	%	30

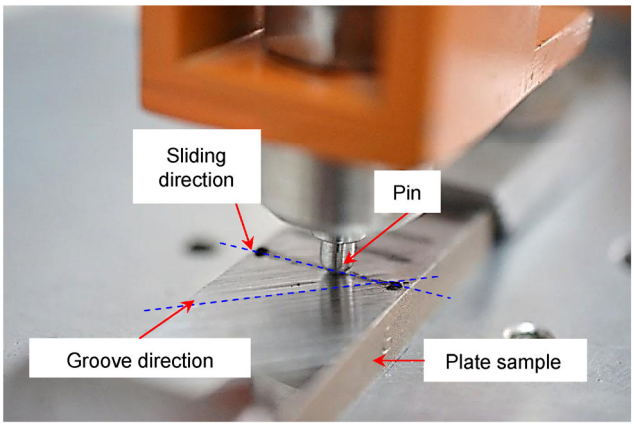

Fig. 6 Test condition of the pin-on-plane.

$$V = \frac{\pi h}{2}\left(r^2 + \frac{h^2}{3}\right) = \frac{\pi h^3}{6} + \frac{\pi h R^2}{2} \quad (1)$$

where:

- R: Radius of the pin
- r: radius of wear track of the pin measured using a Dual beam Nova 600 Nanolab (FEI) scanning electronic microscopy (SEM).
- h: depth of wear track calculated using the following Eq. (2):

$$h = R - \sqrt{R^2 - r^2} \quad (2)$$

3 Results and discussion

3.1 Effect of initial surface topographies on friction coefficient

Figures 8(a) and 8(b) show the friction curves under various topographies of planes at different sliding velocities. The variation of the friction coefficient during the 5,000 cycles under a contact pressure of 1,000 MPa indicates that the orientation of the initial surface roughness affects the friction coefficient. It can be observed that the friction coefficient decreased with the increase of the sliding velocity independently of the topography of the planes surfaces. This result is in good agreement with Koan-Sok et al. [13]. Also, the friction curves can be separated into two stages: "first stage" representing the break-in period and "second stage" stopping at 5,000 cycles where the friction coefficient was stabilized.

The next important observation resulting from Figs. 8(a) and 8(b) would be the effect of continuous and discontinuous contacts at the second stage. Indeed, the friction coefficients of the rough surfaces at 45° and 90° were very close at both the low and the high sliding velocities. This can be explained by the existence of two types of contacts. Figures 9(a) and 9(b) show the continuous contact whereas Figs. 9(c) and 9(d) show the discontinuous contact.

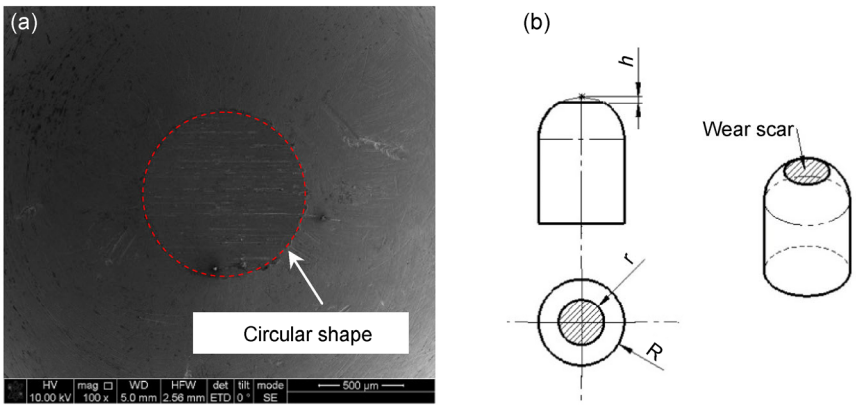

Fig. 7 The pin wear scar (a) SEM observation and (b) schematic form.

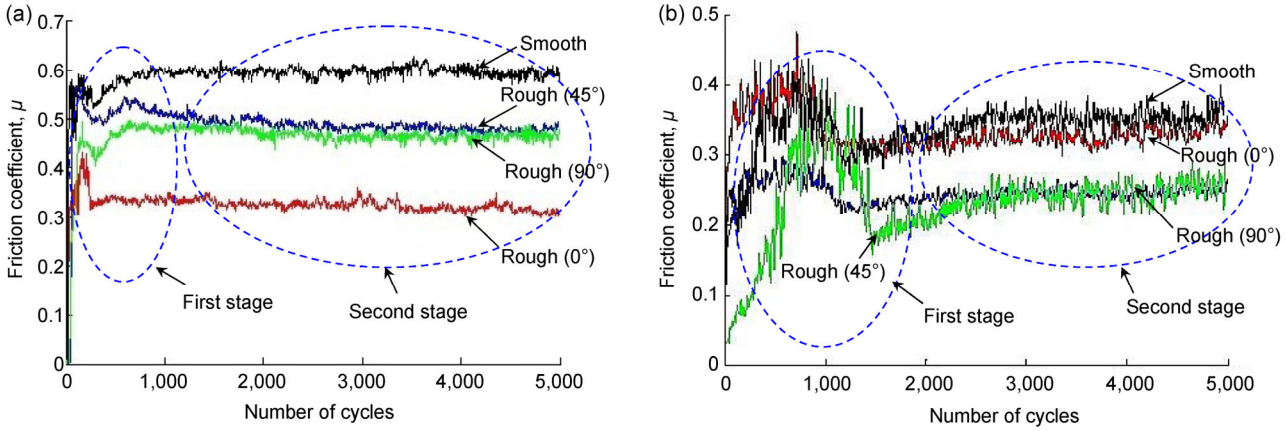

Fig. 8 Friction curves under various initial surface topographies of planes and sliding velocity. (a) 20 mm/s and (b) 80 mm/s.

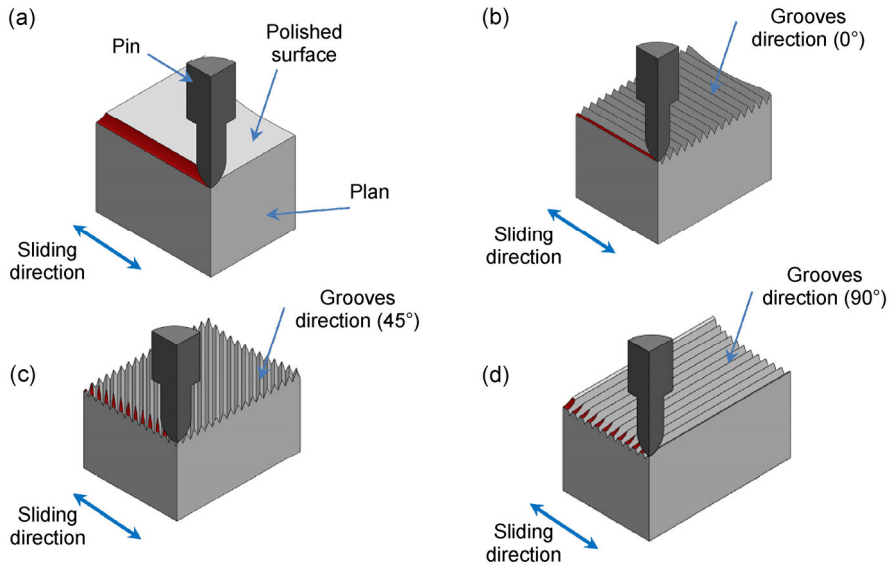

Fig. 9 Simulation of the contact mode. (a) and (b) Continuous contact; (c) and (d) discontinuous contact.

When comparing the different friction coefficients obtained with rough surface, Fig. 9 clearly shows that the highest friction coefficient was obtained with grooves oriented at 45°. This can be explained by the effect of debris ejection [16]. Indeed, Cartier and Kapsa revealed that the orientation of the grooves parallel to the orientation of the sliding causes less friction because they do not trap debris. Hence, 45° or 90° grooves would trap more debris and cause a higher friction coefficient. Moreover, Colombié et al. [17] argued that trapped debris form an oxide bed that raises the friction coefficient. Our findings confirmed these observations.

Figure 10 presents the mean values of the friction coefficient with error bars corresponding to the standard deviations of the three repeated tests within each surface topography and under two sliding velocities, 20 mm/s and 80 mm/s. It is clear that the friction coefficient for all rough surfaces was lower than that for the smooth surfaces. In the second stage and with a sliding velocity at 80 mm/s, the friction coefficient with the rough surface planes 45° and 90° yielded the same value of friction coefficient. This friction coefficient was 0.25. However, both the smooth and the rough surface planes at 0° yielded the same maximum friction coefficient of 0.32.

It can be easily observed that the smooth surface provided the maximum contact surface and generated the maximum adhesion force. This resulted in yielding the maximum friction coefficient. This finding was

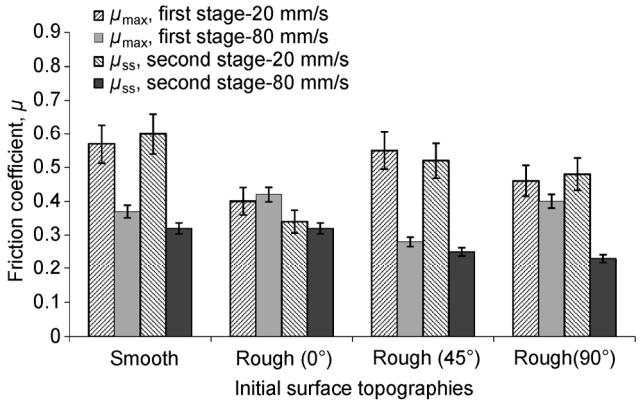

Fig. 10 Friction coefficient (μ_{max} and μ_{ss}) under different initial surface topographies.

in total agreement with previous works [16, 18]. Nevertheless, grinding surfaces with 0°, 45° and 90° groove orientations, the contact surface area was minimal compared to that between pin and smooth plane. The presence of asperities in the rough plane shown in Fig. 4, would be behind the reduction of the contact area. This result confirms previous findings [19, 20]. Indeed, Sedlacek et al. [19] who used a pin-on-disc tribometer found that the friction coefficient of a polished surface had a higher value than a rough surface. Equally, Xie and Williams who used a pin-on-cylinder tribometer found similar results [20]. They demonstrated the reduction of the roughness value greatly increased the friction coefficient.

Using the break-in curves model Fig. 11 [21, 22] can determine the stabilization of the friction coefficient in function of the type and number of cycles necessary to reach the μ_{ss} value.

Table 4 illustrates the duration of the break-in and the type of coefficient curve at 20 mm/s and 80 mm/s sliding velocity and under surfaces topographies. The shape differences of the curves can be explained by the fact that the stabilization of the friction coefficient depends on the sliding velocity and the surface topographies of planes. When the sliding velocity is low, the maximum number of cycles to bring the coefficient curve to stabilization is about 1,000 cycles. This value was observed with a rough plane surface at 45° orientation. However the maximum number of cycles to get stabilization was multiplied two times at a high sliding velocity of 80 mm/s. The maximum of 2,000 cycles was obtained with rough surface planes having grooves oriented at 90°. However, only the test with a rough surface plane oriented at 0° showed a friction curve having an unchanged curve pattern independently of the sliding velocity. Three break-in curve shapes were observed after friction tests, types (b), (c), and (d). According to Peter [22] the shape of the curve type (b) can be explained as follows: the initial roughness of the surface produces a momentary rise in friction until the surface reaches conformity. Then, smoothing occurs and the friction is reduced. The drop after the initial peak can also be due to the surface texturing by shear, or by the development of a low-shear transfer film.

The shape of the curve type (c) can be considered an indicator of the effect of temperature. Indeed, several previous works have established the fact that

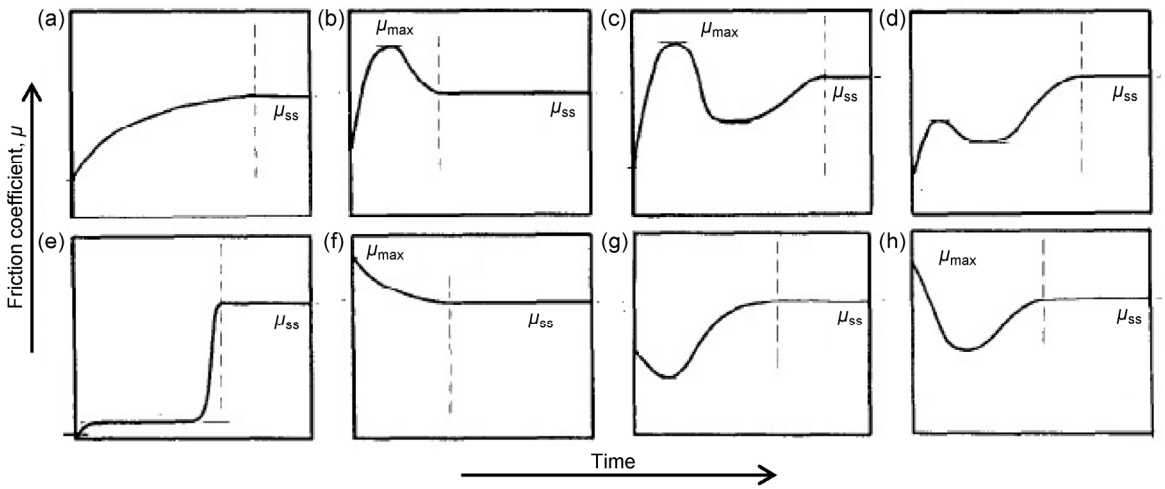

Fig. 11 Types of break-in curve shapes.

Table 4 Break-in data for pin-on-plane tests.

Initial surface topographies	Sliding velocity 20 mm/s		Sliding velocity 80 mm/s	
	Type of break-in	Number of cycles to μ_{ss}	Type of break-in	Number of cycles to μ_{ss}
Smooth	(d)	700	(c)	1,800
Rough 0°	(b)	250	(b)	1,000
Rough 45°	(c)	1,000	(b)	1,200
Rough 90°	(d)	850	(c)	2,000

the increase of the sliding velocity increases the temperature between the contact surfaces [11, 23]. In this study, it was observed that the temperature increased fourfold when the velocity increased yielding the break-in curve shape type (c) and the increase of the break-in period. The shape of the curve type (d) occurred during the break-in lower sliding velocity on smooth and rough surface planes with 90° grooves. In addition, the shape of this curve may be caused by the mechanical disruption of surface oxide films which would increase the contact surface as was explained in previous works [22].

3.2 Wear analysis and surface damage

Figure 12 shows the total wear volume/cycle and the wear volume/cycle of pin just for the first stage. When the sliding velocity was fixed at 20 mm/s, the total wear volume for all pins was lower than the total wear volume obtained with a sliding velocity fixed at 80 mm/s. The initial surface topography was significantly affected with high velocity. When the sliding velocity increased fourfold, the wear volume of pins under rough surfaces, with orientation grooves 0° and 45°, increased threefold. In addition, the wear volume/cycles ratio in the first stage seemed insignificant compared to that in the second stage. In line with previous works [24], we can explain this finding as follows. At the beginning of the friction test, only asperities were in contact with the pin. Therefore, the material was relatively easily removed under the effect of the pressure surpassing the elasticity of the studied materials. Furthermore, the sliding velocity of 80 mm/s showed a pronounced delamination in the form of micro-cracks at the top side of the roughness picks. In addition, attached delaminated sheets seemed to be completely detached

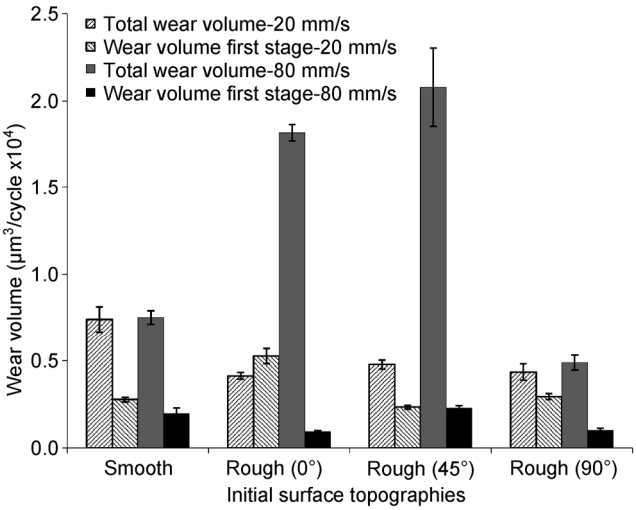

Fig. 12 Variation of the wear volume depending on the surface condition (smooth and rough with 0°, 45° and 90° grooves orientation) and the sliding velocity.

by shear during friction tests. This phenomenon would be responsible for the increase of debris or free wear particles occurring in the process of interaction between the two surfaces. In total agreement with previous works, we can consider these particles as a third body which controls friction and wear via its rheology and flow [16, 17, 25]. It is obvious that the evacuation or the trapping of the debris depends on the surface topography of rail and the sliding direction. Besides, the debris agglomeration would contribute to the increase of friction coefficient and wear value observed above.

Figure 13 shows SEM observations illustrating the presence of many defects in the pin surfaces such as cracks, plastic deformation, incomplete and complete delamination. First, cracks and micro-cracks are clearly seen in different sizes and shapes. Second, the observable plastic deformation of materials in the surface of pins can be interpreted as a sign of surface distortion under high stress. This finding supports Suh's five-step scenario of friction tests [26]. Indeed, this scholar reported a wear particle formation in the delamination wear process under a complex loading and sliding velocity. In the first step of this process, as illustrated by Fig. 13(b), the transmission of normal and tangential load between contact surfaces can lead to a deformation and break of asperities observed under the cyclic stress effect. In the second step of this process, as illustrated by Fig. 13(d), the cyclic motion

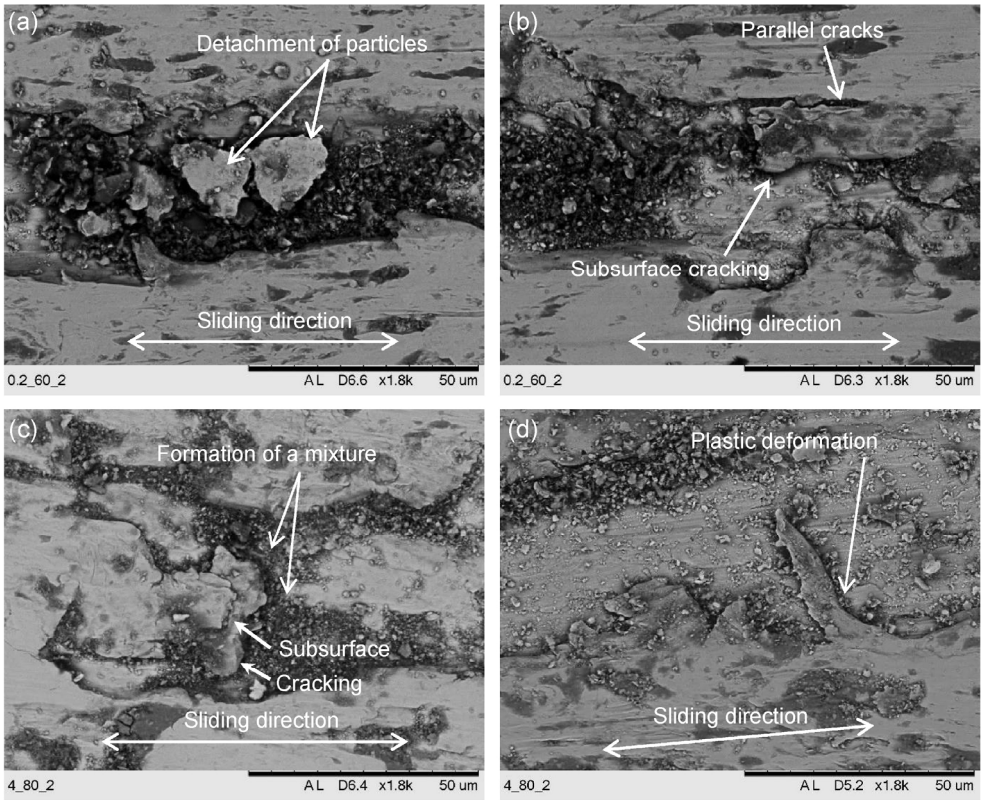

Fig. 13 Pin surfaces damage at sliding velocity 80 mm/s under initial surface topographies. (a) smooth contact; (b), (c) and (d) rough surfaces with different grooves orientations 0°, 45° and 90°, respectively.

of asperities accumulates the stress and deforms the surface plastically by shear. In the third step the cracks are nucleated below the surface (Fig. 13(c)). The fourth step is illustrated by Fig. 13(b). Once the cracks are present, further cyclic stress causes them to extend. These tend to propagate parallel to the surface. The fifth step is illustrated by Fig. 13(a), when the cracks finally shear to the surface long and thin wear sheets delaminate. This study adopted Suh's explanation of the thickness and growth of the wear sheet. Indeed, this scholar rightly argued that the thickness of the wear sheet is controlled by the location of subsurface crack growth, which is controlled by the normal and tangential stress value in the surface [26].

4 Conclusion

In this study, tribological tests of the wheel/rail contact were undertaken with four initial surface topographies: a smooth surface and three different rough planes with groove orientations at 0°, 45° and 90° of the sliding direction. The main objective of this work was to determine possible causes that contribute to premature wear of the wheels. The main findings of this study can be summarized as follows:

First, the initial surface topographies seemed to have a significant effect on the friction coefficient independently of the speed. Second, the increase of the sliding velocity would decrease the friction coefficient. Third, especially when accompanied with a high sliding velocity, an initial rough surface would have a significant effect on the wear of the wheel. Fourth, the highest wear values were observed at groove orientations of 45° when accompanied with a high sliding velocity. Finally, the break-in duration seemed to depend on the initial surface topographies of the rail and the sliding velocity.

Acknowledgement

The authors would like to thank Dr. Ayadi Hajji for his help with proofreading and improving the English

and editing of the manuscript.

References

[1] Eric E M, Joseph K. The application of contact mechanics to rail profile design and rail grinding. *Wear* **253**: 308–316 (2002)

[2] Cuervo P A, Santa J F, Toro A. Correlations between wear mechanisms and rail grinding operations in a commercial railroad. *Tribol Int* **82**: 265–273 (2015)

[3] Rippeth D, Kalousek J, Simmons J. A case study of the effect of lubrication and profile grinding on low rail roll-over derailments at CSX transportation. *Wear* **191**: 252–255 (1996)

[4] Chandrasekar S, Farris T N, Hebbar R R, Hucher S A, Bulsara V H. Thermal aspects of surface finishing process. In *ASM Metals Handbook: Surface Engineering* 5. ACM, 1997: 152– 157.

[5] Lyu Y, Bergseth E, Olofsson U, Lindgren A, Höjer M. On the relationships among wheel-rail surface topography, interface noise and tribological transitions. *Wear* **338**: 36–46 (2015)

[6] Khalladi A, Elleuch K. Tribological behavior of wheel-rail contact under different contaminants using pin-on-disk methodology. *ASME J Tribol* **39**: 011102 (2016)

[7] Sundh J, Olofsson U. Seizure mechanisms of wheel-rail contacts under lubricated conditions using ball-on-disc test method. *Tribol Int* **41**: 867–874 (2008)

[8] Lundmark J, Höglund E, Prakash B. Running-in behavior of rail and wheel contacting surfaces. In *International Conference on Tribology*, Parma, Italy, 2006: 20–22.

[9] Grassie S. Requirements for transverse railhead profile and railhead roughness following grinding. In *6th International Heavy Haul Conference*, Cape Town, South Africa, 1997: 6–10.

[10] Hiensch M, Larsson P-O, Nilsson O, Levy D, Kapoor A, Franklin F, Nielsen J, Ringsberg J W, Josefson B L. Two-material rail development: Field test results regarding rolling contact fatigue and squel noise behaviour. In *6th International Conference on Contact Mechanics and Wear on Rail/Wheel Systems*, Gothenburg, Sweden, 2003: 10–13.

[11] Hernandez F C R, Demas N G, Gonzales K, Polycarpou A A. Correlation between laboratory ball-on-disk and full-scale rail performance tests. *Wear* **270**: 479–491 (2011)

[12] Deters L, Proksch M. Friction and wear testing of rail and wheel material. *Wear* **258**: 981–991 (2005)

[13] Koan-Sok B, Keiji K, Tsunamitsu N. An experimental study of transient traction characteristics between rail and wheel under low slip and low speed conditions. *Wear* **265**: 1417–1424 (2008)

[14] Descartes S, Desrayaud C, Niccolini E, Berthier Y. Presence and role of the third body in a wheel-rail contact. *Wear* **258**: 1081–1090 (2005)

[15] Lewis R, Olofsson U. Mapping rail wear regimes and transitions. *Wear* **257**: 721–729 (2004)

[16] Cartier M, Kapsa P. Usure des contacts mécaniques, Maitrise de l'usure et du frottement, BM 5 068–1.

[17] Colombié C, Berthier Y, Floquet A, Vincent L, Godet M. Fretting: Load carrying capacity of wear debris. *ASME* **106**: 194–201 (1984)

[18] Beek A. Advanced engineering design-lifetime performance and reliability. TU Delft, the Netherlands, 2009.

[19] Sedlacek M, Podgornik B, Vizintin J. Influence of surface preparation on roughness parameters, friction and wear. *Wear* **266**: 482–487 (2009)

[20] Xie Y, Williams J A. The prediction of friction and wear when a soft surface slides against a harder rough surface. *Wear* **196**: 21–34 (1996)

[21] Peter J B. Interpretations of the friction and wear break-in behavior of metals in sliding contact. *Wear* **71**: 29–43 (1981)

[22] Peter J B. On the nature of running-in. *Tribol Int* **38**: 1007–1012 (1977)

[23] Saka N, Eleiche A M, Suh N P. Wear of metals at high sliding speeds. *Wear* **44**: 109–125 (2002)

[24] Kapoor A, Franklin F J, Wong S K, Ishida M. Surface roughness and plastic flow in rail wheel contact. *Wear* **253**: 257–264 (2002)

[25] Descartes S, Saulot A, Godeau C, Bondeux S, Dayot C, Berthier Y. Wheel flange/rail gauge corner contact lubrication: Tribological investigations. *Wear* **271**: 54–61 (2011)

[26] Suh N P. An overview of the delamination theory of wear. *Wear* **44**: 1–16 (1977)

Abdessalem KHALLADI. He received his bachelor degree in mechanical engineering from Higher School of Technical and Science of Tunis (ESSTT), Tunisia, in 2002. He received his MS degree in mechanical engineering from National Engineering School of Sfax (ENIS), Tunisia, in 2011. He joined the Laboratory of Materials Engineering and Environment (LGME) at National Engineering School of Sfax, Tunisia, in 2009. He finalized his Ph.D degree in the same laboratory. His research includes the tribological behavior of wheel and rail materials, mechanical design and manufactory. His current position is a technologist in Higher Institute of Technological Studies of Sfax, Tunisia.

Khaled ELLEUCH. He received his M.S. and Ph.D degrees in material engineering from Ecole Centrale de Lyon, France, in 1998 and 2002, respectively. He joined the Laboratory of Materials Engineering and Environment (LGME) at National Engineering School of Sfax (ENIS), Tunisia, in 2003. His current position is a Professor and Dean of Material Engineering Department. His research areas cover the mechanics of material and durability, material forming, tribology and surface treatment, tribocorrosion and nano-composite development.